Hindawi
Shock and Vibration
Volume 2021, Article ID 1060841, 16 pages
https://doi.org/10.1155/2021/1060841

Research Article

Numerical Evaluation of the Opening Effects on the Reinforced Concrete Slab Structural Performance

Meysam Aminitabar,[1] Omar Kanaani,[2] and Amir Reza Eskenati[3]

[1]*Department of Civil Engineering, K. N. Toosi University of Technology, Tehran, Iran*
[2]*Urban Architecture Engineering, Rojava University of Science and Technology, Chairman Architect Engineering Department, Qamishlo, Syria*
[3]*Strength of Materials and Structural Engineering Department, Polytechnic University of Catalonia, C/Colom 11, TR45, Terrassa 08222, Spain*

Correspondence should be addressed to Amir Reza Eskenati; amir.reza.eskenati@upc.edu

Received 11 August 2021; Revised 7 September 2021; Accepted 15 September 2021; Published 18 October 2021

Academic Editor: Carlo Rosso

A finite element method was used in this study to investigate the effects of openings on the resistive behavior of concrete slabs. The presented modeling procedure is used to conduct numerical analyses on the response of reinforced concrete slab subjected to in-plane monotonic loads in X (perpendicular to the beam) and Z (parallel to the beam) directions. Initially, the developed numerical model was calibrated and compared with laboratory results. In building this three-dimensional model, it is attempted to accurately model all nonlinear properties of steel and concrete materials as well as the interactions between them. Then, the behavior of bilaterally concrete slabs under different loads was investigated and used as a reference. Finally, the effect of openings under different loads on the strength of concrete slabs was studied. The results confirm that openings have a great influence on the change of hardness, ductility, initiation and cracking path, and stress distribution under shear and gravitational loading. Moreover, by adding an opening inside the diaphragm, not only did beam and block flooring show more fragile behavior, but also its strength and resistance decreased against lateral load. Given the results of the parametric study of the effect of layout, generally, its place became critical at the state that opening disturbed transmission of shear stresses to the collector beams. By adding the area of the opening and loading in X direction, the concentration of the tensile stresses (equivalent to main maximum stresses) was at the tensile edge as well as at the middle of the flooring around the opening. It is worth noting that an increase in the opening's area caused the number of tensile stresses to be increased at the middle of the flooring. Meanwhile, the concentration of maximum compressive stresses which is equivalent to the main minimum stresses was at the compressive edge, started at the area of the collectors, and stretched to the edge of the opening. Among different layouts, X-1 and Z-3 states were more critical than other states. Considering openings with different layouts, X-1 and Z-3 have the most stiffness deteriorating and strength in such a way that stiffness deteriorating and strength were 39.93% and 37.89%, respectively, for Z-3 model and 38.68% and 43.33%, respectively, for Z-3 model.

1. Introduction

Reinforced concrete (RC) slabs supported by RC columns are among the frequently used structural systems. The specific abilities of this system make them applicable alternatives for the construction industry. So, several studies about their simulation have been performed and design methods are proposed. Besides their advantages, RC slab-columns systems have their own weakness in punching shear caused by brittle failure mode. To control punching shear failure, particular attention must be paid to design and implementation [1, 2]. Many national and international construction codes have been investigated and several methods were introduced for calculating and implementing such systems [3]; fib Bulletin 14 [4]; Italian guide CNR DT200 [5]; Japan Society of Civil Engineers (JSCE) design recommendations [6]. By examining these codes, it can be stated that they are actually studying the same subject and

the difference in expression is due to the different point of view [7]. Using bonded rebar in a concrete slab is a common method to increase the punching shear strength of the RC slab-column systems [8, 9]. Furthermore, the inevitable presence of openings in these systems because of architectural and structural considerations makes the task of evaluating safe performance more complicated [10]. Hence, many analytical studies, numerical researches, and experimental efforts have been done on the performance evaluation of RC slab subjected to many various different loading types [11, 12]. Most scholars believe that rebar-concrete interaction in RC slab can be simulated with the assumption of the perfect bond at the interface between them [13, 14]. Some researchers investigate the effect of bonding-debonding in simulating the structural performance of RC slabs [15, 16].

Finally, in 2016, Khajehdehi and Panahshah [17] conducted studies on the effect of openings on the in-plane structural behavior of RC floor slabs and concluded that the collapse mechanism of slabs with an opening significantly differed from the mechanism of slab collapse without opening. Furthermore, the presence of openings in floor diaphragms for architectural features, staircases, and elevator shafts is sometimes inevitable [18]. These openings will result in diaphragm stiffness reduction and can decrease the load-carrying capacity of the member [19, 20]. These types of diaphragms are usually designed to ignore opening effects. Therefore, their true response may be different from what is assumed. In other words, the presence of openings makes the behavior of floor diaphragms significantly more complicated and unpredictable [21]. A number of researchers have evaluated the structural behavior of RC slabs with openings in them. However, slabs were only subjected to out-of-plane gravity loads, and the effect of in-plane loads was not considered [22–25]. A number of researchers have evaluated the structural behavior of RC slabs with the presence of opening and out-of-plane loading. Radik et al. [26], Choi et al. [19], and Floruț et al. [21] studied the effect of various strengthening methods on improving the load-bearing capacity of slabs with the presence and absence of openings using FRP, GFRP, and FRC [27]. Khajehdehi and Panahshah conducted a numerical study of the effect of the opening on the floor slab concluding that the presence of an opening plays an important role in determining the behavior of the slab plates [17].

In this study, debonding of rebar from concrete surfaces is taking into account. It is obvious that validated FE simulations may cause accurate results on the response of RC slabs. Also, it is obvious that, in numerical studies, one should use logical assumptions to get closer to the finite element model that the numerical models of reinforced concrete slabs are no exception. Until now, most studies have focused on the behavior of unilateral reinforced concrete slabs, and more limited studies have been conducted on the impact of openings on the structural performance of bilateral concrete slabs [28, 29]. So far, many studies have been carried out on this issue due to the high capability of such a structural system. However, the number of comprehensive studies that have modeled and investigated the purely nonlinear behavior of materials coupled with the precise definition of the interaction between its components is limited. Thus, the 3D nonlinear finite element model of RC slab considering the rebar-concrete interaction is used to simulate such structural elements [30]. In a structure, the need for an opening in the roof system (slab) for architectural features, stairs, elevator shafts, pipelines, and utility ducts is inevitable. These openings will in some status lead to a decrease in the stiffness of the roof system and collapse load due to their dimensions relative to the dimensions of the slab [19, 31]. In designing these types of slabs, the effects of openings are usually ignored. Therefore, their actual response may be different from that assumed. Radik et al. [26], Choi et al. [19], and Floruț et al. [21] investigated the effectiveness of different strengthening methods on improving the load-carrying capacity of slabs with and without openings using GFRP, FRC, and FRP, while slabs were only subjected to out-of-plane loads and again the effect of in-plane loads was not considered. Zhang et al. [32] conducted a numerical study on the effect of openings on floor slabs and concluded that the presence of openings plays an important role in determining the in-plane behavior of the slabs. In the present research, a two-way RC slab system tested by Durucan and Anil is used to validate the numerical fully nonlinear FE model [33].

The main scope of the performed numerical this study is the simulation of direct and indirect impact of horizontal construction openings on expected structural functions of bilateral reinforced concrete slabs. In this regard, the influence of different positions and sizes of openings on the deformation and hardness of reinforced concrete slabs is studied in detail and the results are compared with each other to obtain a comprehensive view.

2. Material and Methods

2.1. Benchmark Experimental Study (Durucan and Anil [33]). In this study, the shear behavior of the slab interior connection in addition to FRP reinforced opening with bar was studied using a set of experiments. In this study, a sample without an opening and 8 other samples with openings were along the sides and diagonal. In all samples, slab dimensions have been $2000 \times 2000 \times 120$ mm and bar dimensions were 200×200 mm as shown in Figure 1. In this research, Durucan and Anil's modeling in ABAQUS finite element software was used due to the lack of valid experimental researches on beam and block floorings. Then after results' confirmation, a model was provided and studies of flooring were designed for beam and block according to Iran's regulation for finite element software [34].

During the experiment, a hydraulic jack on the column imposes a fixed axial load on the column which is indicative of the gravity load obtained from the frame analysis [35]. In this set of experiments on the compressive strength of concrete, all samples were selected in the range of 21.45–19.78 MPa. Steel strength features and compressive strength are presented in Tables 1 and 2, respectively.

Meanwhile, the way the experiment is conducted is indicated schematically as shown in Figure 2. In this experiment, a concrete reinforced slab was placed on IPE steel pieces and then a hydraulic jack imposed axial load to the column [36].

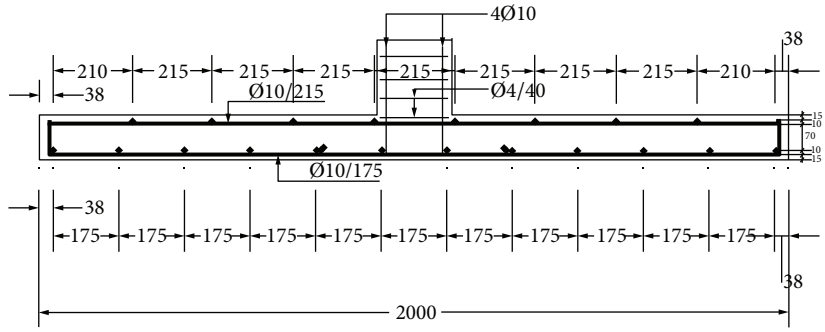

Figure 1: Arrangement of slab reinforcement (dimensions in mm) [33].

Table 1: Features of the steel materials [33].

Reinforcement diameter (mm)	Yield strength (MPa)	Ultimate tensile strength (MPa)	Type
4	280	427	Plain
10	537.34	3838.20	Deformed

Table 2: Features of the concrete used in the samples [33].

Spec. number	Concrete compression strength f_c (MPa)	Opening	
		Size (mm)	Location
1	20.83	Reference (without opening)	
2	20.56	300 × 300	Parallel (adjacent of column)
3	19.96	300 × 300	Diagonal (adjacent of column)
4	21.23	500 × 500	Parallel (adjacent of column)
5	19.78	500 × 500	Diagonal (adjacent of column)
6	20.12	300 × 300	Parallel 300 mm far from column
7	21.45	300 × 300	Diagonal 300 mm far from column
8	20.03	500 × 500	Parallel 300 mm far from column
9	21.09	500 × 500	Diagonal 300 mm far from column

Table 3 shows the experimental results. As it can be seen, the displacement in the sample without opening is 40 mm toward the center which is equivalent to 193 kN [37].

3. Nonlinear 3D FE Analyses

3.1. Numerical Validation Process

3.1.1. Common Component Modeling of the Samples. For all samples, model geometry including components such as concrete slab, reinforcements, and rigid supports and loading in the software separately, as shown in Figure 3, were modeled, and finally, the samples were made completely in the software by putting these components along each other. Since constraints and interactions among the components have a great influence on the results of the analysis, it was applied carefully and cautiously.

3.1.2. Types and Sizes of the Elements. The concrete column was modeled by three-dimensional elements accessible at the library of numerical software [38]. The concrete slab was meshed using C3D8R elements as shown in Figure 4. Reinforcements and supportive components were modeled using T3D2 and C3D8R truss elements, respectively. Dimensions of the elements were considered as 20 mm for slab and steel reinforcements and 100 mm for support (see Figure 4).

3.1.3. Interaction and Constraints Conditions among Different Components. Where concrete contacts steel, the surface-to-surface constraint was used without friction coefficient which is shown in Figure 5 (contact of supportive sheets with concrete slab). For the rigid sheets, a point that is called reference point is defined too that all degrees of freedom for these sheets are affected by this point. A Tie constraint is defined; when two surfaces adhere to each other, one should be determined as Master surface and another as Slave surface. As it is mentioned in the software manual, it is better that the surface which has finer materials be determined as a Slave surface and the dimensions of its elements be smaller than those of the Master surface in order to avoid numerical errors. Therefore, when the constraint is used, points' displacement of the Slave surface is obtained through the points' displacement of the Master surface and indeed relative slip between these two surfaces is neglected.

3.1.4. Boundary Conditions. In laboratory tests, the connection of the support is to fixed ground. Therefore, in its modeling in the software, all rotational and transitional degrees of

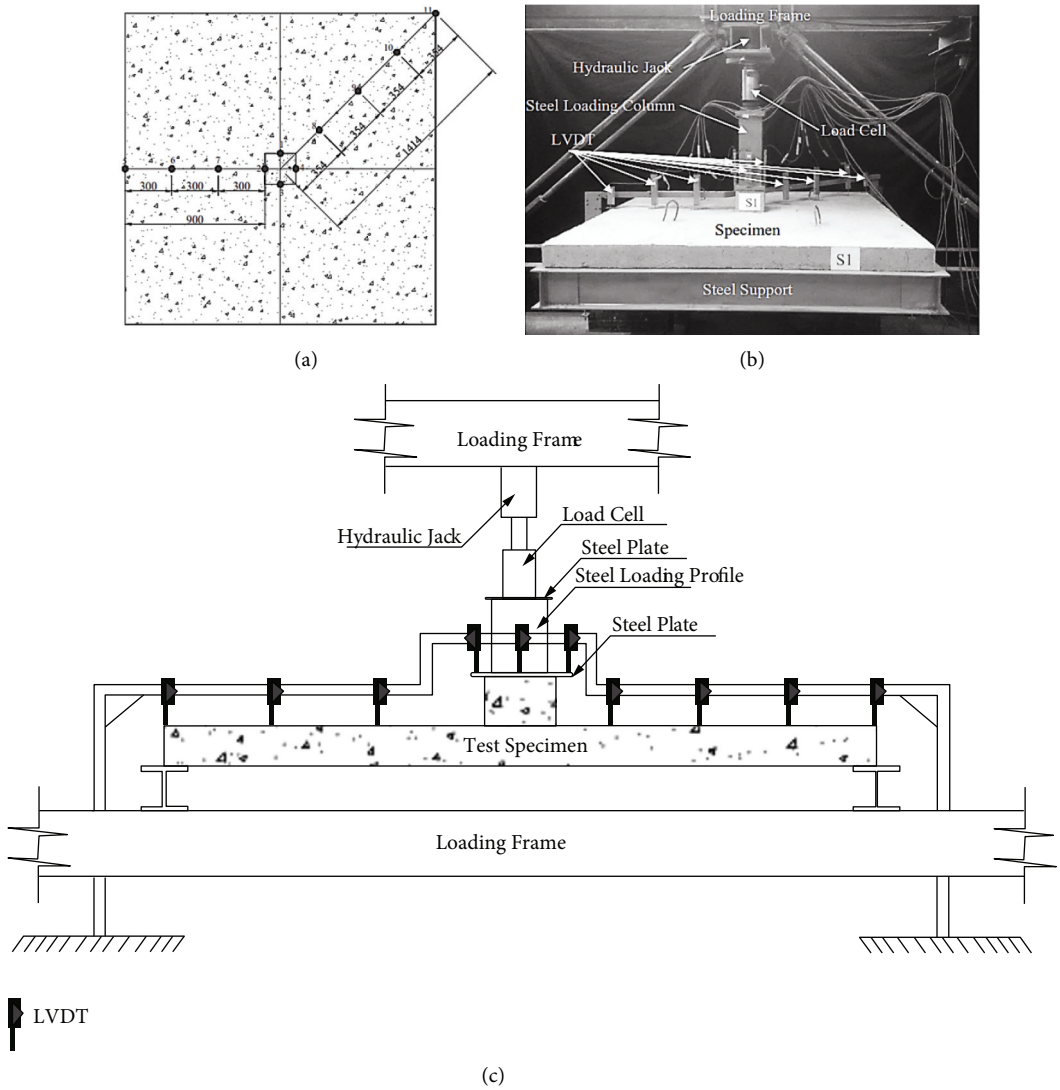

Figure 2: Reinforced concrete slab test layout [33]. (a) Location of strain gauges. (b) Schematic figure of the experiment. (c) The manner in which the experiment is conducted.

Table 3: Results of the experiment [33].

Spec. number	Ultimate Load (kN)	Load ratio	Disp. (mm)	Disp. ratio	Max. disp. (mm)	Max. disp. ratio	Initial stiffness (kN/mm)	Initial stiffness ratio	Energy dissipation (kN·mm)	Energy dissipation ratio	Max. strain (mV)
1	193.03	1.00	37.47	1.00	37.99	1.00	60.43	1.00	4595.87	1.00	—
2	161.18	1.63	35.41	1.96	45.66	1.16	95.49	8.23	4466.50	2.11	6554
3	186.08	1.48	40.17	1.50	49.82	1.49	152.38	11.41	5685.90	2.38	5001
4	157.71	2.05	32.26	1.42	40.09	0.91	78.16	8.65	3664.40	2.68	5245
5	173.31	1.83	36.52	0.88	45.81	1.01	49.33	4.86	4574.20	2.22	4965
6	197.42	1.46	42.13	1.19	52.88	1.22	61.95	5.06	7155.30	1.95	5136
7	219.36	1.27	43.67	1.15	55.57	1.16	69.15	3.69	7293.00	1.77	4332
8	190.86	1.65	51.06	1.11	62.63	1.19	48.84	4.10	7326.20	2.45	4513
9	201.84	1.45	39.93	1.19	42.61	0.98	55.54	3.21	5071.80	1.30	3546

freedom U_1, U_2, U_3, UR_1, UR_2, and UR_3 are closed. In the laboratory test, a hydraulic stimulant was conducted which keeps the column at its current situation before starting the test and only allows it to rotate around the sheet. In the software, also UR_3 is kept open to simulate degrees of freedom. Sides around the slab can move up, down, and round inside the sheet.

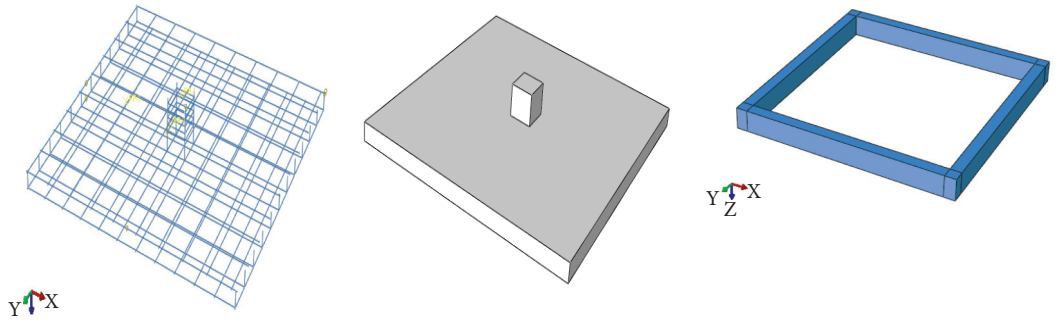

(a) (b) (c)

Figure 3: Different components of slab. (a) Longitudinal and transverse reinforcement. (b) Concrete slab and column. (c) Slab support.

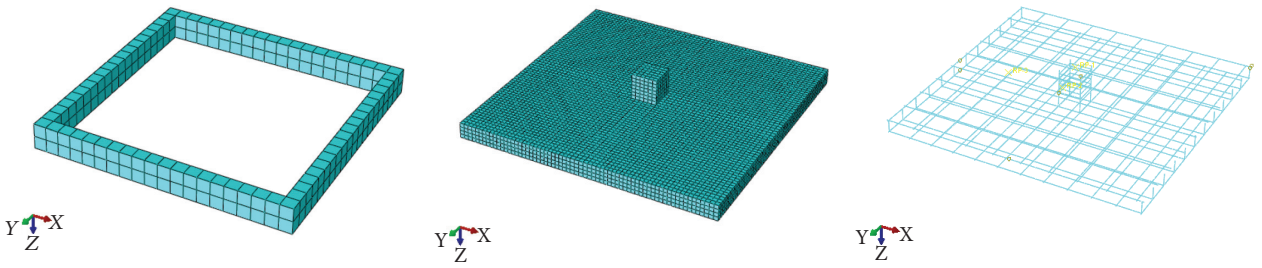

(a) (b) (c)

Figure 4: 3D finite element model of RC slab. (a) Determination of the elements of support. (b) Meshing of the concrete slab. (c) Meshing of the steel reinforcements.

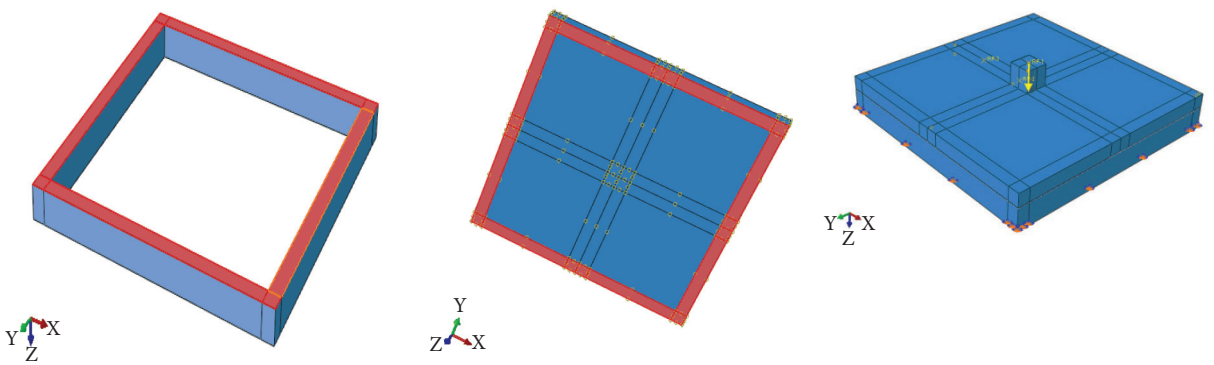

(a) (b) (c)

Figure 5: 3D FEM interaction and loading. (a) Master surface. (b) Slave surface. (c) Axial load place.

3.1.5. Comparing Experimental Results and Numerical Outputs. At first, finite component samples were studied and validated to be sure that intended samples are modeled correctly and the given parameters have reasonable values, it was seen that the numerical results and laboratory results are in good agreement, and then a series of parametric studies were conducted to investigate the efficacy of different components of the connection. Figure 6 shows the comparison of the force-displacement response of the finite element method with the experimental method.

As it can be seen from Figures 6(a) and 6(b), the results of numerical analysis and laboratory results are in good agreement, indicate completely identical behavior, and experience the maximum strength at nearly 40 mm, but at displacements higher than this amount, strength decreased due to concrete cracking. Figure 7 compares concrete slab cracking in the experimental study and numerical model. It can be seen that most cracks are observed in the area in the middle of the concrete slab.

3.2. Numerical Analysis of Bidirectional Concrete Slab

3.2.1. FEM of Reinforced Concrete Slabs. To provide a model for beam and block flooring, concrete slab and steel truss were modeled in ABAQUS software as shown in Figure 8. As

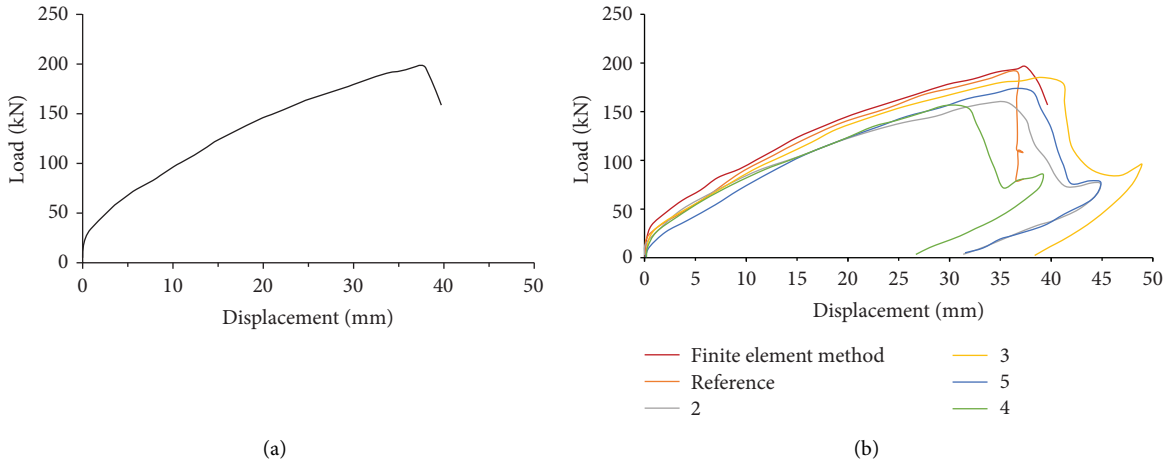

Figure 6: Comparison of the force-displacement response of the finite element method (in red) with the experimental method. (a) FEM result. (b) Experiment result [33].

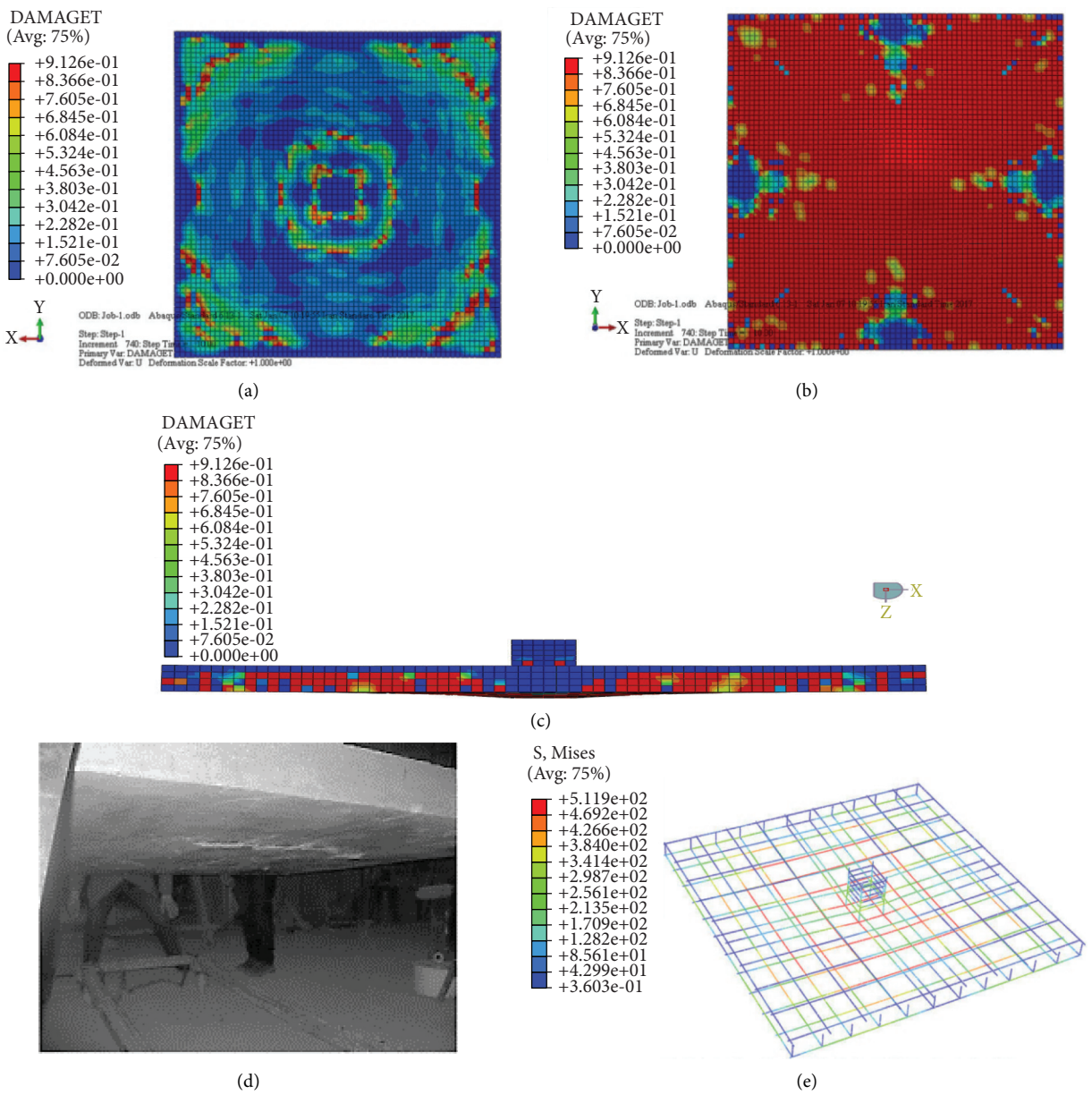

Figure 7: Numerical model validation results. (a) Cracks on the top of the concrete slab. (b) Cracks on the bottom of the concrete slab. (c) Side view of cracked concrete slab. (d) Concrete slab cracking at laboratory model. (e) Stress distribution in slab reinforcements.

shown in this figure, the concrete component was modeled as solid and mashed with C3D8R elements. This element was a hexagonal 8-node one and reduced integration was used in it. Reinforcements were modeled as wire and were meshed with two-node three-dimensional truss elements (T3D2). Dimension for each element was considered 20 mm.

3.2.2. Loading and Boundary Condition for Numerical Model. Since the cross section of the model was different in two X and Z directions, all analyses were done in two directions. Boundary conditions of the model were applied in the way that transitional degrees of freedom were closed at two edges of the slab which means for analysis in X direction and for analysis in Z direction in two edges of the slab, $U_x = U_y = U_z = 0$. Therefore, a volumetric load was applied incrementally with a linear trend. Applied load to the diaphragm was very higher than the regulatory amount. The cause for the higher load applied is to allow the diaphragm to pass linear area and enter to plastic range in order to study its behavior carefully. Boundary conditions and how models were loaded in two X and Z directions are indicated in Figure 9.

3.2.3. Studying the Diaphragm Behavior in the Numerical Model without Opening. By applying lateral body force, distribution of main maximum plastic strains (see Figure 10) which is equivalent to cracking strains is in such a way that, by loading in direction in the model, crack expansion is perpendicular to the direction of loading and cracking is more in the place of the beam to slab connection. Meanwhile, the rupture mechanism is completely visible in the area where it plays the role of tensile, due to the existence of axial force. Meanwhile, cracks at the support's areas are sheering which is less dominant in Figure 10 because the section of the diaphragm of this mechanism is strong.

Meanwhile, in the model of loading in Z direction, crack distribution is centered more in the collector area which is because the diaphragm section is small in this direction. Meanwhile, after terrible cracks in the collector area, crack expansion was obliquely towards inside the diaphragm and these cracks penetrated more deeply at the collector area. It is worth mentioning that, as shown in Figure 10, in the models with loading in X and Z directions, the maximum amount for main maximum plastic strains which is equivalent to cracking strain is 0.02561 and 0.1041, respectively. It means that, in this area, cracks were opened widely due to the weakness of the diaphragm section to bear the loading direction. Of course, this amount of strain for far displacement of 15 mm is not far-fetched.

Figure 11 shows the distribution of the main minimum plastic strain (equivalent to corrosion strains) from the strain in maximum strength; in the model with volumetric loading in X direction, distribution of corrosion is focused on the connection points of the beams to slab. Meanwhile, as it is clear on compression chord, strains are purely compressive. Meanwhile, cracks at the support's areas are sheering which are less dominant in Figure 11(a) because the diaphragm section is strong. Meanwhile, in the model with loading in Z direction, the distribution of corrosion strains of the concrete was more concentrated at the collector area because the section of the diaphragm is small in this direction as shown in Figure 11(b) too. It should be noted that the expansion of corrosion was less than cracking which can be seen clearly by comparing Figures 10 and 11.

Meanwhile, the distribution of main maximum and minimum stresses at displacement equivalent to maximum strength for models with loading in Z and X directions is shown in Figures 12 and 13 which indicate the stress transmission mechanism in the diaphragm in these two directions. As it is clear in these figures, the mechanism of collector bars and chord is clearly visible and the highest stress was created in these places. Therefore, bars located in these areas can tolerate the forces resulting from the mechanism and collectors.

3.2.4. Reaction of Lateral Force-Displacement of Diaphragm without Opening. Force applied to the diaphragm linearly and incrementally was extracted against transformation at the middle of the opening by the software. The amount of this force against the transformation of the middle point of the slab is indicated in Figure 14.

As shown in Figure 14, the behavior of diaphragm with beam and block section in Z direction in the direction of beam's axis, bean, and block flooring indicated more fragile behavior which is mainly because of the weakness of the diaphragm in stress transmission at the collector area. The amounts of maximum force, displacement equivalent to maximum force, and hardness of the diaphragm are indicated in Table 4.

3.3. Numerical Study of Opening Effects on RC Slab. There is no doubt that the existence of voids inside the diaphragm can affect the capacity to create lateral force in the diaphragm. The area and location of the opening are things that its critical place on the diaphragm performance and the amount of stress created inside it and especially around the opening should be determined. Particularly, investigating these parameters at beam and block flooring as the most common details in Iran has great importance. In this section, the location of the opening and its area at this kind of flooring has been studied parametrically.

3.3.1. Modeling Hypothesis of the Opening in Diaphragm. In order to model the opening, the opening model was created by creating a square opening inside it in the way that both slabs and reinforcements were cut. Meanwhile, due to the complexities of modeling, the hypothesis of not slipping the reinforcements inside the concrete was considered by taking embedded region interaction into account. Meanwhile, no reinforcement was used around the opening. Similar to the previous section, loading on the diaphragm model in addition to opening was conducted and studied in two Z and X directions. For parametric studying, firstly the layout of the opening was studied, then the most critical

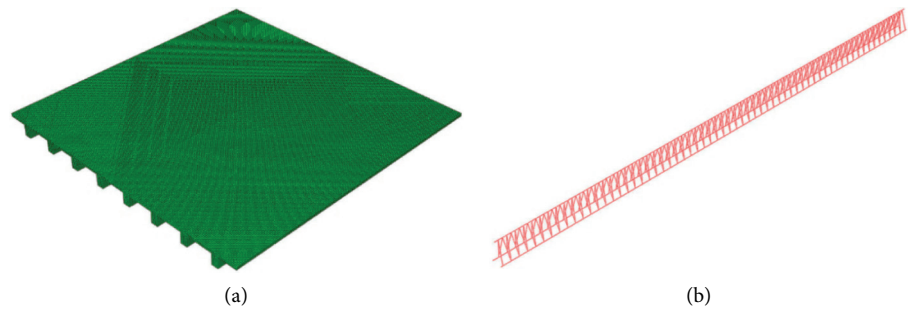

(a) (b)

Figure 8: Bidirectional concrete slab finite element model. (a) Set of concrete elements. (b) Steel truss used in joists.

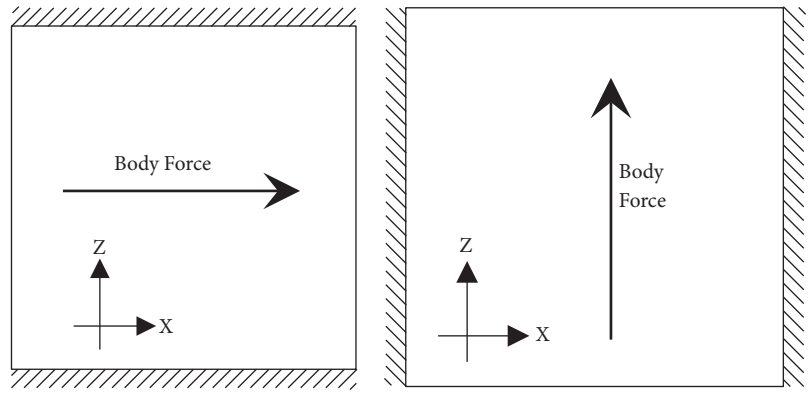

(a) (b)

Figure 9: Boundary condition and loading. (a) Boundary and loading conditions in X direction. (b) Boundary and loading conditions in Z direction.

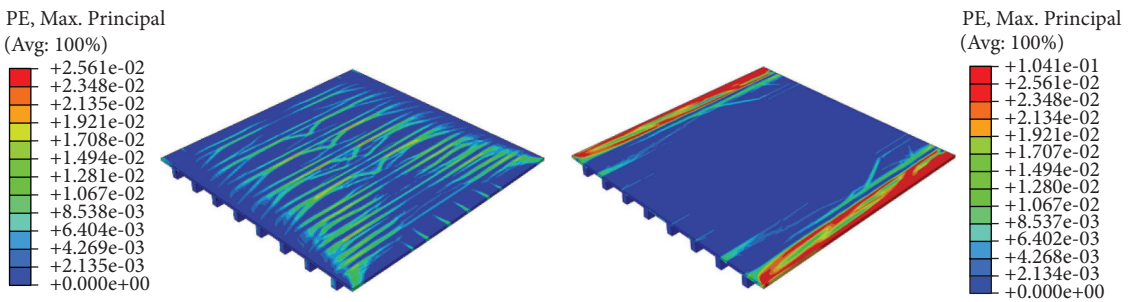

(a) (b)

Figure 10: Distribution of main maximum plastic strain which is equivalent to cracking strain at concrete slab at 15 mm displacement. (a) Distribution of tensile cracks in the model by loading in X direction. (b) Distribution of tensile cracks in the model by loading in Z direction.

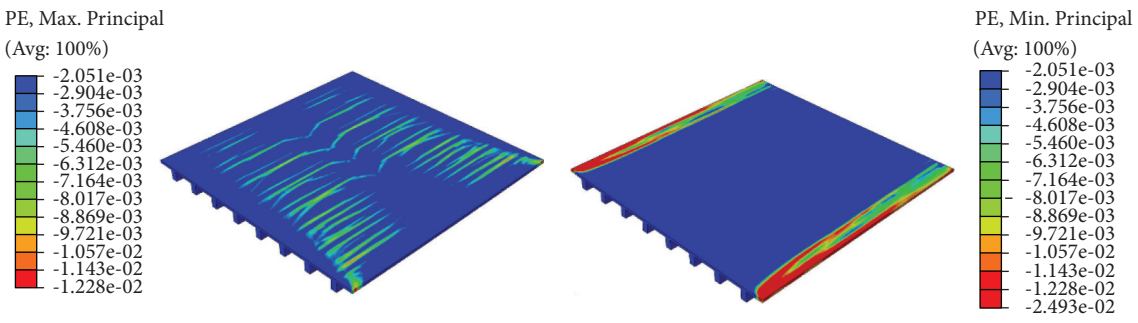

(a) (b)

Figure 11: Distribution of cracks caused by corrosion in the concrete slab at 15 mm displacement. (a) Distribution of cracks caused by concrete crushing in the model with X-ray loading. (b) Distribution of cracks caused by concrete crushing in the model with Z direction loading.

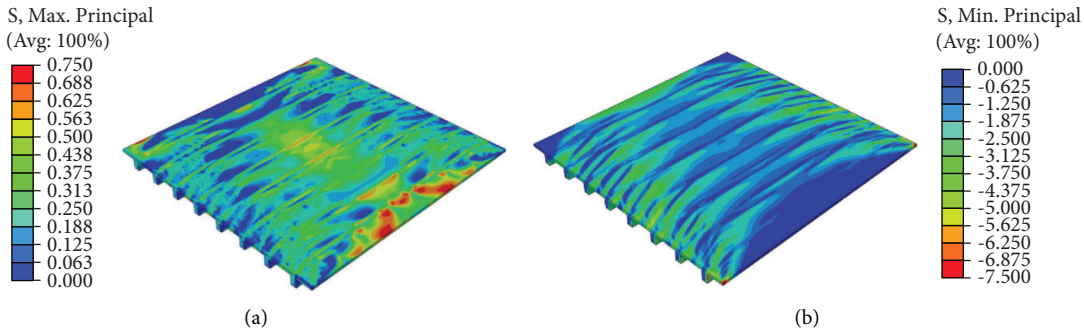

Figure 12: Distribution of main maximum and minimum stresses for a model with loading in X direction (MPa) at displacement equivalent to maximum strength. (a) Maximum principal stress distribution in concrete slab (MPa). (b) Distribution of minimum stress in concrete slab (MPa).

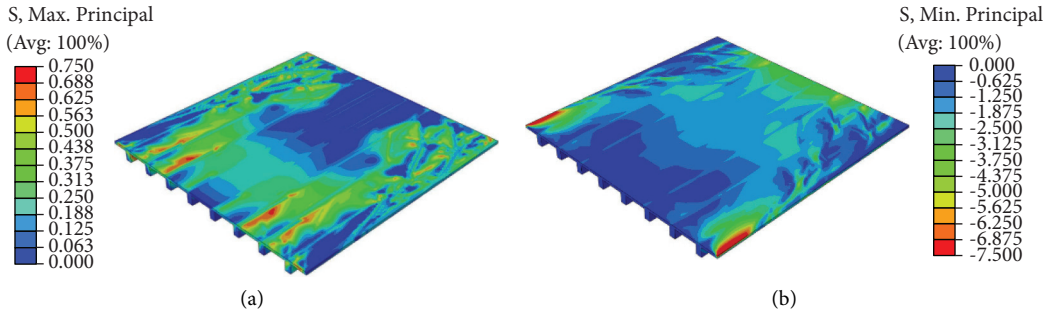

Figure 13: Distribution of main maximum and minimum stresses for a model with loading in Z direction (MPa) at displacement equivalent to maximum strength. (a) Maximum principal stress distribution in concrete slab (MPa). (b) Distribution of minimum stress in concrete slab (MPa).

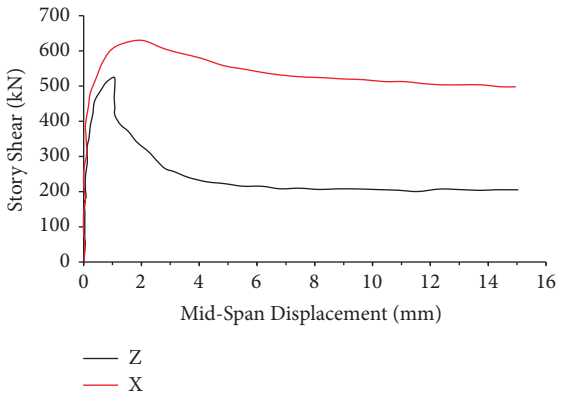

Figure 14: Floor shear chart against displacement at the middle of diaphragm' opening.

place for the opening was determined, and at the same critical place, the area of the opening was analyzed.

3.3.2. Parametric Study of the Opening Layout inside Diaphragm of Beam and Block Flooring. To model the layout of opening at the diaphragm, a square opening of 2 m × 2 m was used which is equivalent to 16% of the diaphragm. The location of the opening and the name of the corresponding model have been shown in Figure 15. What is worth mentioning in Figure 15 is that, considering symmetry, X-4, X-5, and X-6 models can be ignored at the loading state in X direction as these models are, respectively, correspondent with X-2 and X-8 models. Meanwhile, at the state of loading in Z direction, Z-6, Z-7, and Z-8 models can be neglected as they are correspondent to Z-2, Z-3, and Z-4 due to being symmetric.

Applied force to the diaphragm, which was applied linearly and incrementally, was extracted against the transformation of the middling of the opening through software. The amount of this force against the transformation of the slab's middle point is shown in Figure 16(a) for the models with loading in X direction and in Figure 16(b) for the models with loading in Z direction.

By comparing charts of Figures 16(a) and 16(b), it can be found that, by adding the opening inside the diaphragm of the beam and block flooring, not only does diaphragm show more fragile behavior but also its strength and hardness decrease against lateral force too. Meanwhile, it can be clearly seen by comparing these two figures that loading diaphragm in Z direction shows more fragile behavior. In such a way that, after reaching the diaphragm to its maximum capacity, it is accompanied by a sudden decrease in strength. Meanwhile, by comparing Figures 16(a) and 16(b) more closely, the results indicated in Tables 5 and 6 can be observed.

For more tangible and accurate study of the critical state for the place of the diaphragm, values calculated for stiffness deteriorating and strength are provided in Tables 5 and 6 as well as in the bar charts drawn in Figures 17(a) and 17(b).

Table 4: Reaction of lateral force-displacement of the diaphragm without opening.

Diaphragm drift at maximum resistance (mm)	Maximum resistance (kN)	Stiffness (kN/mm)	Model name
1.74	629.71	3401.50	X
1.00	537.34	3838.20	Z

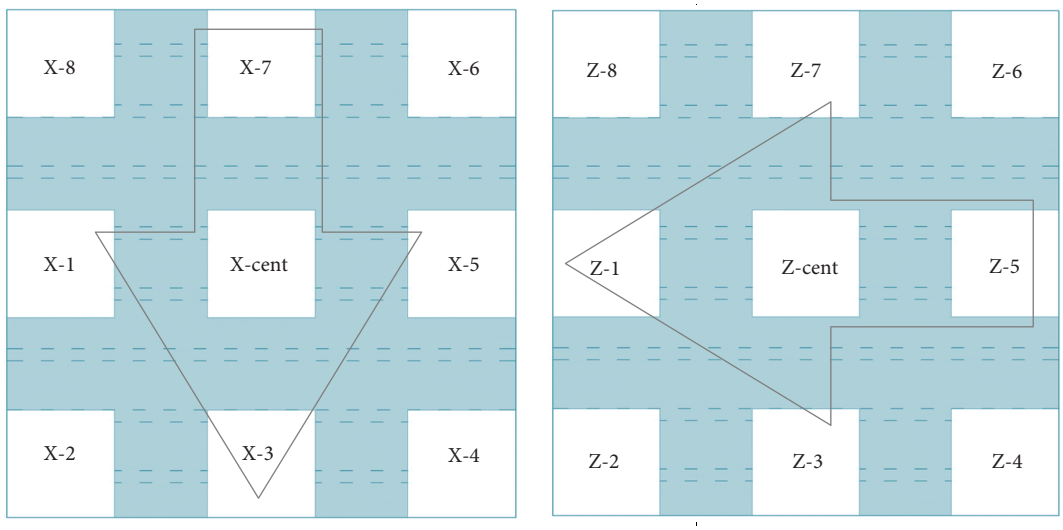

Figure 15: Location of the opening and name of the correspondent model for loading in Z directions. (a) Pop-up location of the corresponding model name for loading in X direction. (b) Pop-up location of the corresponding model name for loading in Z direction.

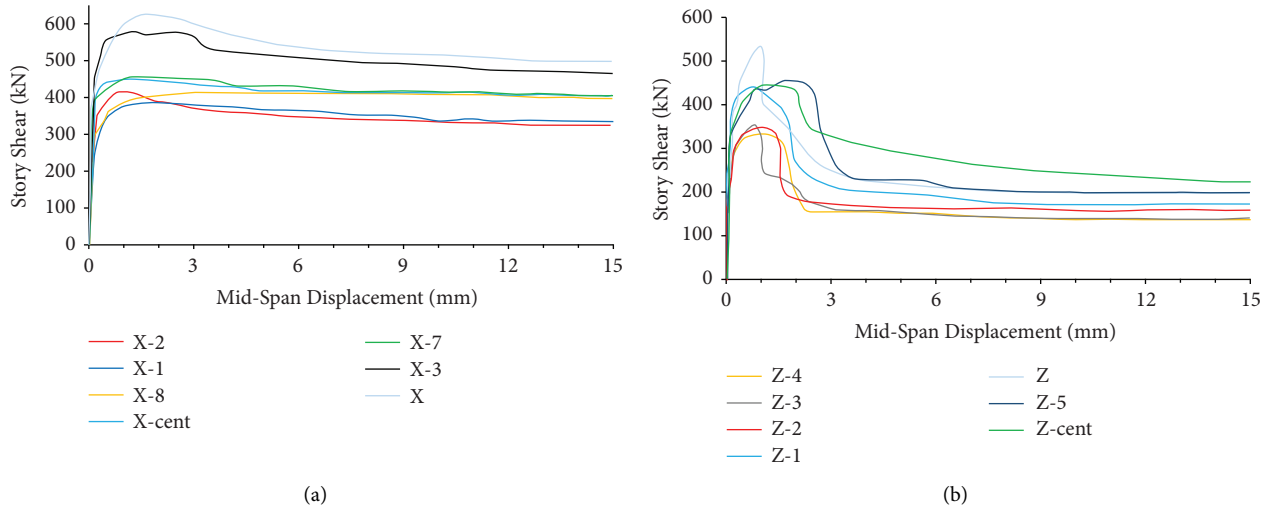

Figure 16: Floor shear chart against displacement in the middle of diaphragm opening for models with opening with different layouts with loading in various directions. (a) Loading in X direction. (b) Loading in Z direction.

As it can be seen from Figures 17(a) and 17(b), X-1 and Z-3 models have the highest stiffness deteriorating and strength which are more critical compared to other models. Meanwhile, the criticality of this opening layout from stress and strain distribution can be seen in the next session. According to the results of the parametric study, opening layout location is critical in two loading modes in X and Z directions, when the opening disrupts the shear stress transfer path to the collector beams. Meanwhile, the X-1 and Z-3 modes are more critical than the others. This is due to the high degree of deterioration and diaphragm resistance shown in Tables 5 and 6 as well as Figure 17.

3.3.3. Parametric Study of the Openings with Various Areas inside Diaphragm of Beam and Block Flooring. In order to investigate the effect of diaphragm area on hardness,

Table 5: Obtained parameters from models with opening with different layouts with loading in X direction.

Deterioration of resistance (%)	Deterioration of stiffness (%)	Diaphragm drift at maximum resistance (mm)	Maximum resistance (kN)	Stiffness (kN/mm)	Model name
—	—	1.74	929.71	3401.58	X
27.59	13.90	1.39	455.99	2928.78	X-cent
37.9	39.93	1.61	391.10	2043.31	X-1
33.34	37.46	1.02	419.74	2127.19	X-2
7.32	9.48	1.31	583.59	3078.87	X-3
27.04	8.70	1.41	459.47	3105.42	X-7
33.94	29.19	2.98	415.98	2408.55	X-8

Table 6: Obtained parameters from models with opening with different layouts with loading in Z direction.

Deterioration of resistance (%)	Deterioration of stiffness (%)	Diaphragm drift at maximum resistance (mm)	Maximum resistance (kN)	Stiffness (kN/mm)	Model name
—	—	1.00	537.34	3838.20	Z
16.00	14.36	1.35	451.37	3286.98	Z-cent
16.95	7.70	0.77	446.28	3542.72	Z-1
34.53	38.95	1.09	351.88	2334.45	Z-2
38.63	43.33	0.83	329.48	2175.71	Z-3
37.21	28.36	0.86	337.40	2749.62	Z-4
14.36	6.38	1.72	460.16	3593.22	Z-5

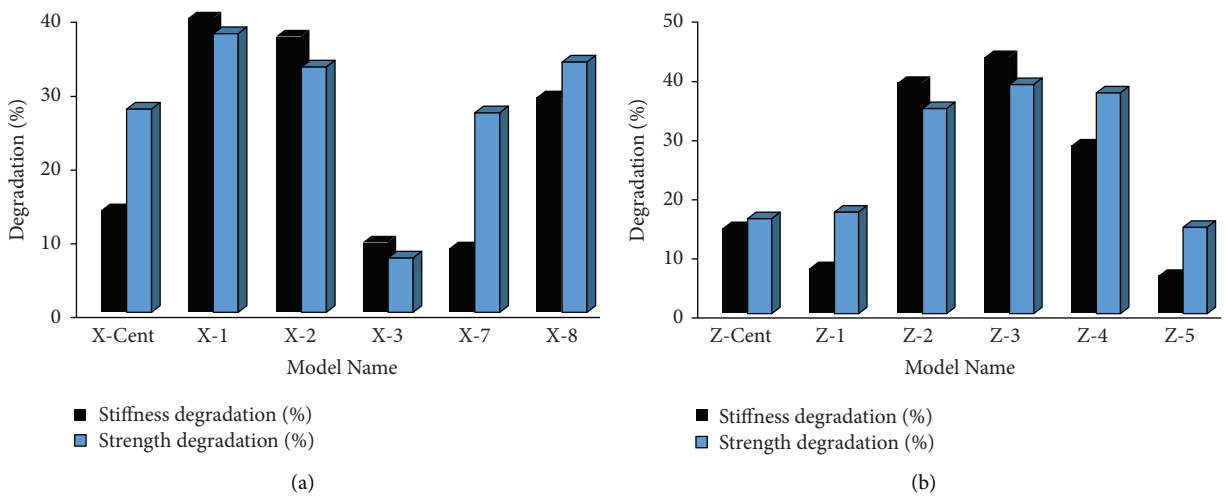

Figure 17: Chart of stiffness deteriorating percentage and ultimate strength for models with opening with loading in various directions. (a) Loading in X direction. (b) Loading in Z direction.

strength, stress transfer mechanisms, cracking and crushing, different critical areas of opening were investigated at these critical locations. The names of these models and how they are applied to the models are shown in Figure 18.

The force applied to the diaphragm linearly and incrementally was extracted from the software against its midspan deformation. The magnitude of this force versus slab midpoint deformation for models with loading in X direction is shown in Figure 19 and for models with loading in Z direction in Figure 20.

It can be seen that, by increasing the area of the opening inside the diaphragm, its resistance and hardness against lateral load decrease. It is also apparent by comparing the two shapes that the Z-diaphragm loading shows a slower and more brittle behavior. So once the diaphragm reaches its maximum capacity, there is a sudden drop in resistance. A closer look at Figures 19 and 20 shows the results in Tables 7 and 8.

In order to more accurately and precisely investigate the effect of the increase of the opening area on the final diaphragm hardness and resistance, the calculated values for the stiffness and resistance decline shown in Tables 7 and 8 are shown in Figure 21.

As can be seen from the previous figures, the diaphragm resistance and stiffness decrease with increasing opening area in numerical models. For models with loading in X direction, the hardness and strength

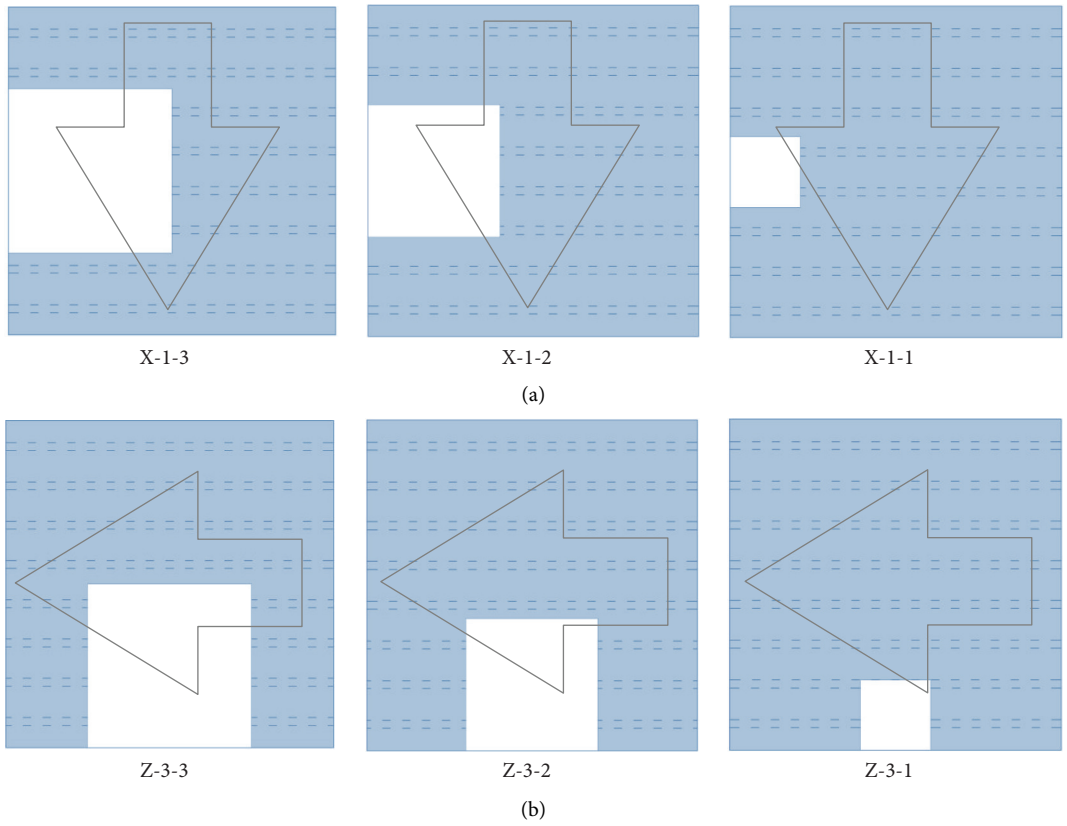

Figure 18: Opening location and corresponding model name for loading in X and Z directions. (a) Opening location and corresponding model name for loading in X direction. (b) Opening location and corresponding model name for loading in Z direction.

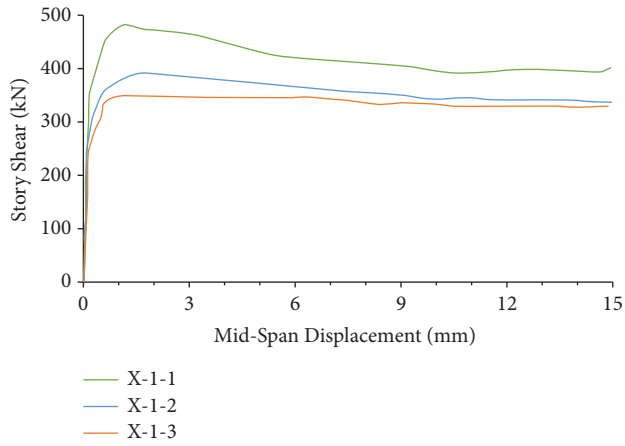

Figure 19: Diagram of story shear versus midspan displacement for models with different opening area under loading in X direction.

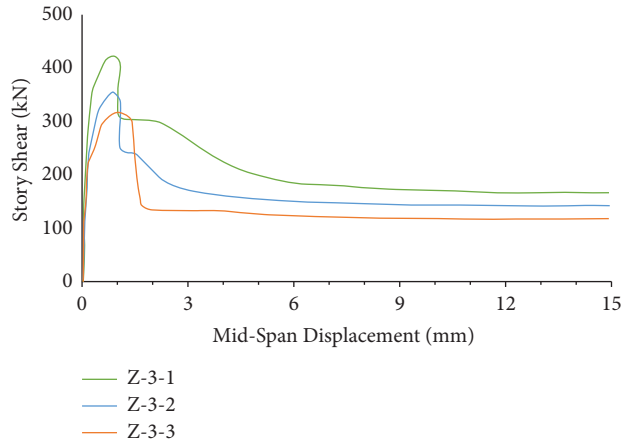

Figure 20: Diagram of story shear versus midspan displacement for models with different opening area under loading in Z direction.

Table 7: Obtained parameters and results from models with opening with different areas under loading in X direction.

Deterioration of resistance (%)	Deterioration of stiffness (%)	Diaphragm drift at maximum resistance (mm)	Maximum resistance (kN)	Stiffness (kN/mm)	Opening ratio	Opening size	Model name
—	—	1.74	629.71	3401.51	—	—	X
23.54	23.96	1.23	481.49	2586.52	4.5	1.06 × 1.06	X-1-1
37.89	39.93	1.61	391.10	2043.31	16	2.00 × 2.00	X-1-2
44.59	43.50	1.89	348.95	1922.02	25	2.50 × 2.50	X-1-3

Table 8: Obtained parameters and results from models with opening with different areas under loading in Z direction.

Deterioration of resistance (%)	Deterioration of stiffness (%)	Diaphragm drift at maximum resistance (mm)	Maximum resistance (kN)	Stiffness (kN/mm)	Opening ratio	Opening size	Model name
—	—	1.00	537.34	3838.20	—	—	Z
18.22	23.07	0.83	422.63	2952.81	4.5	1.06 × 1.06	Z-1-1
33.01	43.33	0.83	329.48	2175.18	16	2.00 × 2.00	Z-1-2
34.72	53.21	0.96	318.69	2042.40	25	2.50 × 2.50	Z-1-3

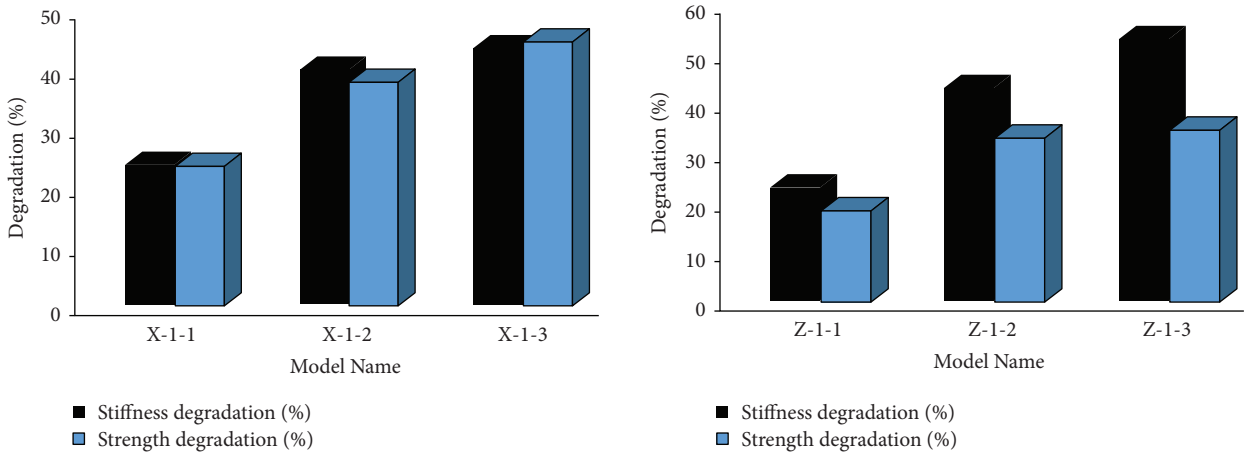

Figure 21: Chart of stiffness deteriorating percentage and ultimate strength for models with opening under loading in X and Z directions.

deterioration rates are approximately the same, but for models with loading in Z direction, the hardness deterioration is greater than the resistance deterioration.

4. Conclusion

In this study, the finite element method was used for three-dimensional modeling and nonlinear analysis on the diaphragm of the beam and block flooring. Meanwhile, the following conclusions are arrived at by studying this kind of diaphragm, with and without opening considering different layouts. By applying volumetric lateral force, distribution of main maximum plastic strains which are equivalent to cracking strains is in a way that, in the model with loading in X direction (perpendicular to the beam), expansion of the crack was perpendicular to the direction of loading. Meanwhile, at the areas that play the role of tensile edge, the rapture mechanism is completely visible due to the existence of the axial force. Meanwhile, cracks at the palace of the support are sheering which is less dominant because the section of the diaphragm is strong. Meanwhile, at the model with loading in Z direction (parallel to the beam), the distribution of the cracking is focused more at the collector area because the section of the diaphragm is small in this direction. Meanwhile, after terrible cracks at the collectors' area, expansion of the crack was obliquely towards inside the diaphragm. Meanwhile, at the area of tensile edge, the distribution of the cracking is completely visible in a tensile manner and the cracks penetrate deeply at the area near to the collectors. At the models with loading in X and Z directions, the maximum amount of main maximum plastic strain which is equivalent to the cracking strain is, respectively, 0.02561 and 0.1041. It means that, due to the weakness of the sections' diaphragm to bear loading in Z direction, this area is forced with the openness of the crack width at a high amount. Of course, this amount of strain is not far-fetched for far displacement of 15 mm for the diaphragm.

By adding an opening inside the diaphragm, not only did beam and block flooring show more fragile behavior but also its strength and resistance decreased against lateral load. Considering the force-displacement charts for the models with opening with different layouts, in which opening is at proximity to the collectors, X-1 and Z-3 have the most stiffness deteriorating and strength in such a way that stiffness deteriorating and strength were39.93% and 37.89%, respectively, for Z-3 model and 38.68% and 43.33%, respectively, for Z-3 model. By studying the distribution of the maximum and minimum plastic strain (equivalent to cracking and corrosion) in the models with opening with different layouts, at loading in X direction, the most cracks occurred at the area in which beams were connected to slab as well as at the corners of the opening. Meanwhile, cracks became critical when the opening was placed in the collectors' area. The distribution of corrosion had been identical to cracking distribution too but its amount was less in the diaphragms. Meanwhile, for the models with loading in Z direction, when the opening was placed in the collectors' area (as the critical state), the most concentration of main maximum plastic strains which was equivalent to cracking was at the collector area. The most concentration of the main minimum plastic strains (equivalent to corrosion) in this state was similar to that at the area of the collector too where the slab tolerated high stresses. The amounts of main minimum plastic strain reached corrosion around the opening proximity to the collector area. Given the results of the parametric study of the effect of layout, generally, its place became critical at the state that opening disturbed transmission of shear stresses to the collector beams. Among them, X-1 and Z-3 states were more critical than other states.

By studying stiffness deteriorating and strength for the diaphragms with the opening with different areas, it was seen that, by increasing the opening area from 0% to 25% area of the diaphragm, stiffness deteriorating and strength increased but the rate of their raising decreased gradually. By studying the distribution of minimum and maximum plastic strain (equivalent to cracking and corrosion) at the models with opening with different layouts, by applying load in X direction to the diaphragm with opening, the most cracking concentrated at the top of the opening and after that at its lower corner by changing the area. Meanwhile, it cracked at the area where the slab was connected to the beams. But it is worth noting at this state of openness that all connections of the beam to slab around the opening are faced with many cracks and corrosion and worsen by increasing the area. The most corrosion was concentrated at the area of tensile edge and at the top of the opening and the highest concentration of main minimum plastic strains which is equivalent to corrosion is around the corners of the opening too. By applying load to the diaphragm with the opening in Z direction, at 15 mm displacement for the diaphragm, the most concentration of main maximum plastic strains, which is equivalent to cracking, was at the area of the collector which was caused due to the weakness of the slab's section at the area connected to the collector beams that slab tolerated high stresses. After that at top of the opening and its lower corner, the main maximum plastic strain arrived at high amounts. Meanwhile, the highest concentration of the main minimum plastic strains equivalent to cracking was at the area of the collectors where slabs bear high stresses. Meanwhile, parts of the opening's corner, which are in the direction of the collectors cracked. It is worth mentioning that, by increasing the opening's area, the amounts of cracking and corrosion increased, and the number of plastic strains became more critical.

Data Availability

The data used to support the findings of this study are available from the corresponding author upon request (amir.reza.eskenati@upc.edu).

Conflicts of Interest

The authors declare that there are no conflicts of interest regarding the publication of this study.

References

[1] I. N. Robertson, T. Kawai, J. Lee, and B. Enomoto, "Cyclic testing of slab-column connections with 272 shear reinforcement," *Structural Journal*, vol. 99, no. 5, pp. 605–613, 2002.

[2] M. H. Harajli and K. A. Soudki, "Shear strengthening of interior slab-column connections using carbon fiber-reinforced polymer sheets," *Journal of Composites for Construction*, vol. 7, no. 2, pp. 145–153, 2003.

[3] R. El-Hacha, "Prestressing concrete structures with frp tendons (aci 440.4 r-04)," in *Proceedings of the Structures Congress 2005: Metropolis and Beyond*, pp. 1–8, New York, NY, USA, April 2005.

[4] K. Pilakoutas, M. Guadagnini, K. Neocleous, and S. Matthys, *The Fib Perspective on FRP Reinforcement in Rc*, FRPRCS-09, Sydney, 2009.

[5] G. Milani, E. Milani, and A. Tralli, "Upper bound limit analysis model for frp–reinforced masonry curved structures. part ii: structural analyses," *Computers & Structures*, vol. 87, no. 23-24, pp. 1534–1558, 2009.

[6] H. Yokota, K. Rokugo, and N. Sakata, "Jsce recommendations for design and construction of high performance fiber reinforced cement composite with multiple fine cracks," *High Performance Fiber Reinforced Cement Composites*, vol. 2, 2008.

[7] M. H. Meisami, D. Mostofinejad, and H. Nakamura, "Punching shear strengthening of two-way flat slabs using cfrp rods," *Composite Structures*, vol. 99, pp. 112–122, 2013.

[8] K. Soudki, A. K. El-Sayed, and T. Vanzwol, "Strengthening of concrete slab-column connections using cfrp strips," *Journal of King Saud University - Engineering Sciences*, vol. 24, no. 1, pp. 25–33, 2012.

[9] A. Stark, B. Binici, and O. Bayrak, "Seismic upgrade of reinforced concrete slab-column connections using carbon fiber-reinforced polymers," *ACI Structural Journal*, vol. 102, no. 2, p. 324, 2005.

[10] B. Binici and O. Bayrak, "Upgrading of slab-column connections using fiber reinforced polymers," *Engineering Structures*, vol. 27, no. 1, pp. 97–107, 2005.

[11] M. B. D. Hueste and J.-W. Bai, "Seismic retrofit of a reinforced concrete flat-slab structure: Part I - seismic performance evaluation," *Engineering Structures*, vol. 29, no. 6, pp. 1165–1177, 2007.

[12] P. Chomchuen and V. Boonyapinyo, "Incremental dynamic analysis with multi-modes for seismic performance evaluation of RC bridges," *Engineering Structures*, vol. 132, pp. 29–43, 2017.

[13] J. Feng, M. Song, Q. He, W. Sun, L. Wang, and K. Luo, "Numerical study on the hard projectile perforation on RC panels with LDPM," *Construction and Building Materials*, vol. 183, pp. 58–74, 2018.

[14] V. K. R. Kodur and A. Agrawal, "Effect of temperature induced bond degradation on fire response of reinforced concrete beams," *Engineering Structures*, vol. 142, pp. 98–109, 2017.

[15] Y. Su, J. Li, C. Wu, P. Wu, M. Tao, and X. Li, "Mesoscale study of steel fibre-reinforced ultra-high performance concrete under static and dynamic loads," *Materials & Design*, vol. 116, pp. 340–351, 2017.

[16] Y. Peng, C. Wu, J. Li, J. Liu, and X. Liang, "Mesoscale analysis on ultra-high performance steel fibre reinforced concrete slabs under contact explosions," *Composite Structures*, vol. 228, Article ID 111322, 2019.

[17] R. Khajehdehi and N. Panahshahi, "Effect of openings on in-plane structural behavior of reinforced concrete floor slabs," *Journal of Building Engineering*, vol. 7, pp. 1–11, 2016.

[18] Ö. Anil, N. Kaya, and O. Arslan, "Strengthening of one way RC slab with opening using CFRP strips," *Construction and Building Materials*, vol. 48, pp. 883–893, 2013.

[19] Y. Choi, I. Park, S. Kang, and C.-G. Cho, "Strengthening of RC slabs with symmetric openings using GFRP composite beams," *Polymers*, vol. 5, no. 4, pp. 1352–1361, 2013.

[20] H. Selim, R. Seracino, E. Sumner, and S. Smith, "Case study on the restoration of flexural capacity of continuous one-way RC slabs with cutouts," *ASCE Journal of Composites for Construction*, vol. 15, no. 6, pp. 992–998, 2011.

[21] S.-C. Floruţ, G. Sas, C. Popescu, and V. Stoian, "Tests on reinforced concrete slabs with cutout openings strengthened with fibre-reinforced polymers," *Composites Part B: Engineering*, vol. 66, pp. 484–493, 2014.

[22] J. Jiangt and A. F. Mirza, "Nonlinear analysis of reinforced concrete slabs by a discrete finite element approach," *Computers & Structures*, vol. 65, no. 4, pp. 585–592, 1993.

[23] O. Enochsson, J. Lundqvist, B. Täljsten, P. Rusinowski, and T. Olofsson, "CFRP strengthened openings in two-way concrete slabs - an experimental and numerical study," *Construction and Building Materials*, vol. 21, no. 4, pp. 810–826, 2007.

[24] P. Casadei, *Assessment and Improvement of Capacity of Concrete Members: A Case for In-Situ Load Testing and Composite Materials*, (Ph.D. Dissertation), University of Missouri- Rolla, Rolla, Missouri, 2004.

[25] H. K. Boon, M. B. Diah, and Y. L. Loon, "Flexural behaviour of reinforced concrete slab with opening," in *Proceedings of the Malaysian Technical Universities Conference on Engineering and Technology (MUCEET)*, Pahang, Malaysia, 2009.

[26] M. J. Radik, E. Erdogmus, and T. Schafer, "Strengthening two-way reinforced concrete floorslabs using polypropylene fiber reinforcement," *Journal of Materials in Civil Engineering*, vol. 23, no. 5, pp. 562–571, 2010.

[27] K. Qin and F. Ma, "Reinforced concrete frame - shear wall structure, floor open hole static finite element analysis," *Advanced Materials Research*, vol. 788, pp. 521–524, 2013.

[28] T. Tsalkatidis and A. Avdelas, "The unilateral contact problem in composite slabs: experimental study and numerical treatment," *Journal of Constructional Steel Research*, vol. 66, no. 3, pp. 480–486, 2010.

[29] B. Chiaia, O. Kumpyak, L. Placidi, and V. Maksimov, "Experimental analysis and modeling of two-way reinforced concrete slabs over different kinds of yielding supports under short-term dynamic loading," *Engineering Structures*, vol. 96, pp. 88–99, 2015.

[30] N. F. Silva Mamede, A. Pinho Ramos, and D. M. V. Faria, "Experimental and parametric 3d nonlinear finite element analysis on punching of flat slabs with orthogonal reinforcement," *Engineering Structures*, vol. 48, pp. 442–457, 2013.

[31] H. M. Seliem, R. Seracino, E. A. Sumner, and S. T. Smith, "Case study on the restoration of flexural capacity of continuous one-way RC slabs with cutouts," *Journal of Composites for Construction*, vol. 15, no. 6, pp. 992–998, 2011.

[32] H. Zhang, D. Jin, and X. J. Zhao, "Reinforced concrete frame - shear wall structure, floor open hole static finite element analysis," *Advanced Materials Research*, vol. 788, pp. 521–524, 2013.

[33] C. Durucan and Ö. Anil, "Effect of opening size and location on the punching shear behavior of interior slab-column

connections strengthened with CFRP strips," *Engineering Structures*, vol. 105, pp. 22–36, 2015.

[34] M. Mastali, M. Mastali, Z. Abdollahnejad, M. Ghasemi Naghibdehi, and M. K. Sharbatdar, "Numerical evaluations of functionally graded RC slabs," *Chinese Journal of Engineering*, vol. 2014, Article ID 768956, 20 pages, 2014.

[35] Y. Gong, Y. Ma, G. Tan, H. Bi, Y. Pang, and C. Ma, "Experimental study and numerical simulation on failure process of reinforced concrete box culvert," *Advances in Civil Engineering*, vol. 2020, Article ID 5423706, 13 pages, 2020.

[36] S. M. S. Kolbadi, H. Piri, A. Keyhani, S. M. S. Kolbadi, and M. Mirtaheri, "Seismic performance evaluation of slotted-web and bolt-flange plate moment connection," *Earthquakes and Structures*, vol. 20, no. 6, pp. 655–667, 2021.

[37] M. Barkhori, S. Maleki, M. Mirtaheri, M. Nazeryan, and S. M. S. Kolbadi, "Investigation of shear lag effect on tension members fillet-welded connections consisting of single and double channel sections," *Structural Engineering & Mechanics*, vol. 74, no. 3, pp. 445–455, 2020.

[38] Z. Wang, L. Cao, F. Ubertini, and S. Laflamme, "Numerical investigation and design of reinforced concrete shear wall equipped with tuned liquid multiple columns dampers," *Shock and Vibration*, vol. 2021, Article ID 6610811, 19 pages, 2021.